Peptide Hydrolysis by the Binuclear Zinc Enzyme Aminopeptidase from *Aeromonas proteolytica*: A Density Functional Theory Study

Shi-Lu Chen,[†,‡] Tiziana Marino,[§] Wei-Hai Fang,[‡] Nino Russo,*[,§] and Fahmi Himo*[,†]

Department of Theoretical Chemistry, School of Biotechnology, Royal Institute of Technology, AlbaNova SE-10691 Stockholm, Sweden, Dipartimento di Chimica and Centro di Calcolo ad Alte Prestazioni per Elaborazioni Parallele e Distribuite-Centro d'Eccellenza MURST, Università della Calabria, I-87030 Arcavacata di Rende (CS), Italy, and College of Chemistry, Beijing Normal University, Beijing 100875, People's Republic of China

Received: October 16, 2007; In Final Form: December 3, 2007

Aminopeptidase from *Aeromonas proteolytica* (AAP) is a binuclear zinc enzyme that catalyzes the cleavage of the N-terminal amino acid residue of peptides and proteins. In this study, we used density functional methods to investigate the reaction mechanism of this enzyme. A model of the active site was constructed on the basis of the X-ray crystal structure of the native enzyme, and a model dipeptide was used as a substrate. It was concluded that the hydroxide is capable of performing a nucleophilic attack at the peptide carbonyl from its bridging position without the need to first become terminal. The two zinc ions are shown to have quite different roles. Zn2 binds the amino group of the substrate, thereby orienting it toward the nucleophile, while Zn1 stabilizes the alkoxide ion of the tetrahedral intermediate, thereby lowering the barrier for the nucleophilic attack. The rate-limiting step is suggested to be the protonation of the nitrogen of the former peptide bond, which eventually leads to the cleavage of the C−N bond.

1. Introduction

Metalloaminopeptidases represent a family of enzymes that use one or two metal ions to specifically cleave the N-terminal amino acid residues of polypeptides and proteins.[1,2] They play fundamental roles in different biochemical events, such as protein maturation and degradation, tissue repair, and cell-cycle control. Aminopeptidase from *Aeromonas proteolytica* (AAP) is a monomeric enzyme (30 kDa) containing two Zn^{2+} ions that are essential for its enzymatic activity.[3−5] AAP exhibits a substrate preference for the hydrophobic N-terminal amino acid residues[6] with a turnover number (k_{cat}) close to 90 s^{-1} for the L-leucine-*p*-nitroanilide substrate at room temperature.[7]

The first X-ray crystal structure of AAP was solved by Cheverier et al. in 1994.[8] Since then, several structures have been deposited,[9−14] including the native enzyme and complexes with various inhibitors. The structures reveal that the active site contains a binuclear zinc center that is bridged by an aspartate (Asp117) and an oxygen species (see Figure 1), which from the high-resolution X-ray structure has been established as a hydroxide ($O_{\mu}H^{-}$).[14] In addition, the two zinc ions are coordinated to the protein via the side chains of His97, Asp179, Glu152, and His256. Glu151, a second-shell residue, is situated very close to the di-zinc core, forming a hydrogen bond to the bridging hydroxide.

On the basis of the crystallographic studies and other kinetic, spectroscopic, and mutational studies, a reaction mechanism (presented in Scheme 1) has emerged for AAP.[7−22]

Once the substrate docks onto the active site with the assistance of a hydrophobic pocket that binds the hydrophobic side chain of the N-terminal residue,[15] the carbonyl group of the peptide bond is proposed to coordinate to Zn1.[10,16,17] Next, the N-terminal amino group binds to Zn2, which induces the bridging hydroxide to become terminal, bound only to Zn1.[7,10,11] The resulting Zn1−OH complex then performs a nucleophilic attack at the carbonyl group, leading to the formation of a tetrahedral gem-diolate intermediate. Next, a proton is transferred from the second-shell Glu151 to the nitrogen, resulting in the breakdown of the tetrahedral intermediate.[13,18] The active site is finally regenerated by releasing the products and binding a new bridging ligand.

Quite recently, quantum mechanical/molecular mechanical (QM/MM) calculations have been used to study the reaction mechanism of AAP.[23] This study gave general support to the mechanism outlined previously. In particular, these calculations confirmed the notion that the bridging hydroxide dissociates and becomes terminal before it can attack the substrate carbonyl. The QM part of the calculations was, however, chosen to be quite large, which only allowed the system to be treated at the semiempirical AM1 level of theory. This drawback thus permitted only a qualitative description of the energetics of the mechanism since the obtained barriers were very high.

In the present work, we used density functional theory (DFT) calculations to investigate the reaction mechanism of AAP. With a model of the active site constructed on the basis of the high-resolution crystal structure (PDB entry 1RTQ),[14] the hybrid functional B3LYP[24] was employed to present a potential energy surface for the reaction and to provide characterization of the transition states and intermediates involved. This approach has previously been successfully applied to study a number of enzyme mechanisms,[25] including a recent study on the mechanism of phosphotriesterase,[25i] which is a related di-zinc enzyme.

* Corresponding authors. E-mail: (N.R.) nrusso@unical.it and (F.H.) himo@theochem.kth.se.
† Royal Institute of Technology.
‡ Beijing Normal University.
§ Università della Calabria.

10.1021/jp710035j CCC: $40.75
Published on Web 02/05/2008

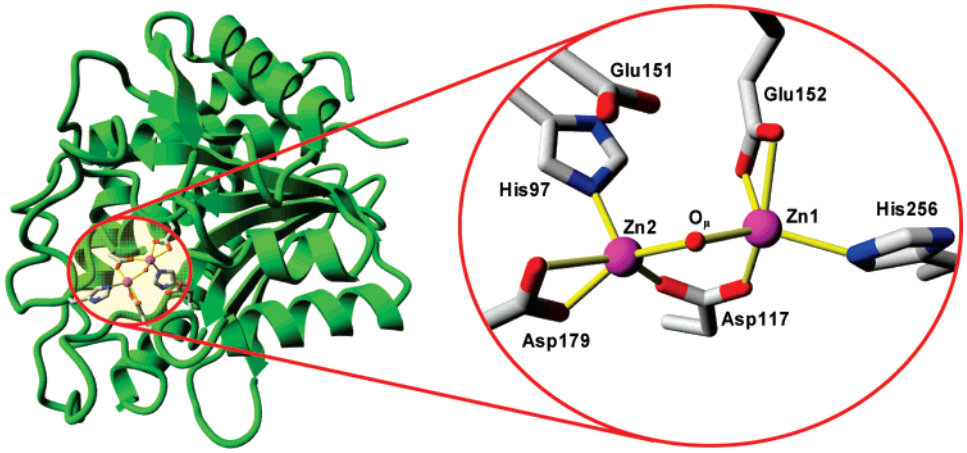

Figure 1. Overall structure of AAP and close-up view of the active site. Coordinates from PDB entry 1RTQ were used to generate the images.[14]

SCHEME 1: Reaction Mechanism for AAP Previously Proposed Based on Experimental and Theoretical Work

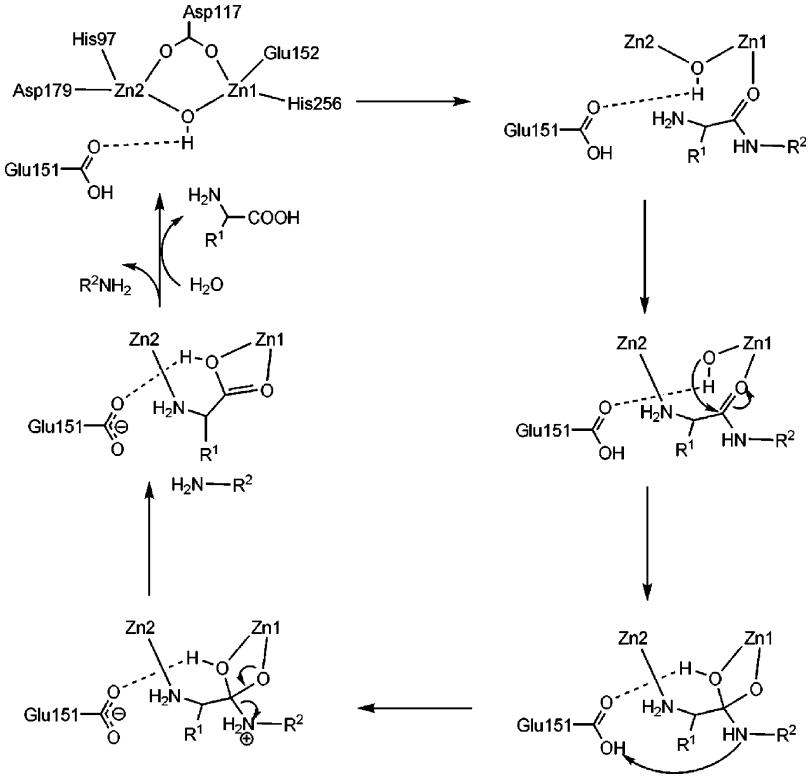

2. Computational Methods

All calculations were performed using the DFT functional B3LYP,[24] which is composed of Becke's three-parameter hybrid exchange functional (B3) and the correlation functional of Lee, Yang, and Parr (LYP). Geometry optimizations were carried out with the 6-31G(d,p) basis set for C, H, O, and N elements and the effective core Stuttgart/Dresden basis set (SDD) for Zn.[26] On the basis of these geometries, more accurate energies were obtained by performing single point calculations with the larger basis set 6-311+G(2d,2p) for all elements. To estimate the energetic effects of the protein environment, solvation effects were calculated at the same theory level as the optimizations by performing single point calculations on the optimized structures using the IEF-PCM method.[27] The dielectric constant (ϵ) was chosen to be 4, which is the standard value used in modeling protein surroundings. Frequency calculations were performed at the same theory level as the optimizations to obtain zero-point energies (ZPE) and to confirm the nature of the stationary points. The latter implies no negative eigenvalues for minima and only one negative eigenvalue for transition states. As will be discussed next, some atoms were kept fixed to their X-ray crystal positions. This procedure gives rise to a few small imaginary frequencies, typically on the order of $10i$ cm^{-1}. These frequencies do not contribute significantly to the ZPE and thus can be tolerated. The energies reported here are corrected for both solvation and zero-point vibrational effects. All calculations were performed using the Gaussian 03 program package.[28]

3. Results and Discussion

3.1. Active Site Model. A model of the active site of AAP was constructed on the basis of the crystal structure of the native enzyme (PDB entry 1RTQ).[14] The model contains the two zinc ions along with their ligands His97, Asp179, Glu152, and His256 and the bridging Asp117 and hydroxide ($O_\mu H^-$). The important second-shell Glu151 was also included. Hydrogen atoms were added manually, and the amino acids were truncated

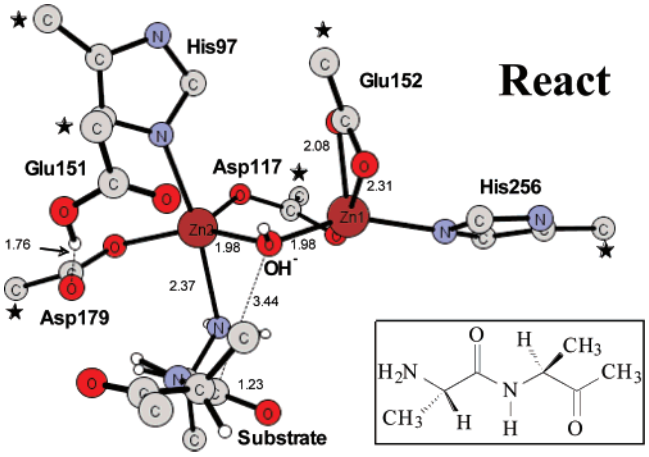

Figure 2. Optimized structure of the AAP active site with the model substrate bound. For clarity, unimportant hydrogen atoms were omitted, which was also applied to other optimized structures. Stars indicate the atoms that are fixed to their X-ray positions. Inserted is the model substrate used in the calculations. All distances are in angstroms.

so that in principle only side chains were kept in the model. The histidines were thus represented by methyl-imidazoles, aspartates and glutamates by acetates. The atoms where the truncation was performed were kept fixed to preserve the spatial arrangement of the residues. These centers are indicated by stars in the figures. As a substrate, we chose a simple model of a di-alanine peptide (see Figure 2). The C-terminus of the dipeptide was blocked with a methyl group to avoid artificial interactions of the carboxyl group with the active site. The total number of atoms in the model is 82, and the total charge is zero.

On the basis of previous results of experimental and theoretical work,[11,14,23] some assumptions have been made about the protonation states of the various groups. The amino terminus of the substrate is assumed to be neutral, the bridging ligand is a hydroxide, and the Glu151 residue is in the protonated form. Glu151 was protonated in the starting structure, consistently with its proposed role of activating the bridging water by abstracting a proton.[18]

The optimized structure of the AAP active site with the model substrate bound, referred to as **React**, is shown in Figure 2. The overall geometric parameters obtained from the geometry optimization agree quite well with the X-ray structure. For example, the bond distances of the bridging oxygen (O_μ) to the two zinc ions are calculated to be 1.98 Å, as compared to the crystallographic distances of 2.00 and 1.94 Å.[14] The computed Zn1−Zn2 distance (3.31 Å) is in excellent agreement with the crystallographic distance of 3.33 Å.[14]

It is interesting to note that, in the reactant structure, the amino group of the substrate binds to the Zn2 ion (Zn2−N distance is 2.37 Å), while there is no interaction between Zn1 and the peptide bond oxygen. A possible reason for this could be that Glu152 binds to Zn1 in a bidentate fashion, making coordination

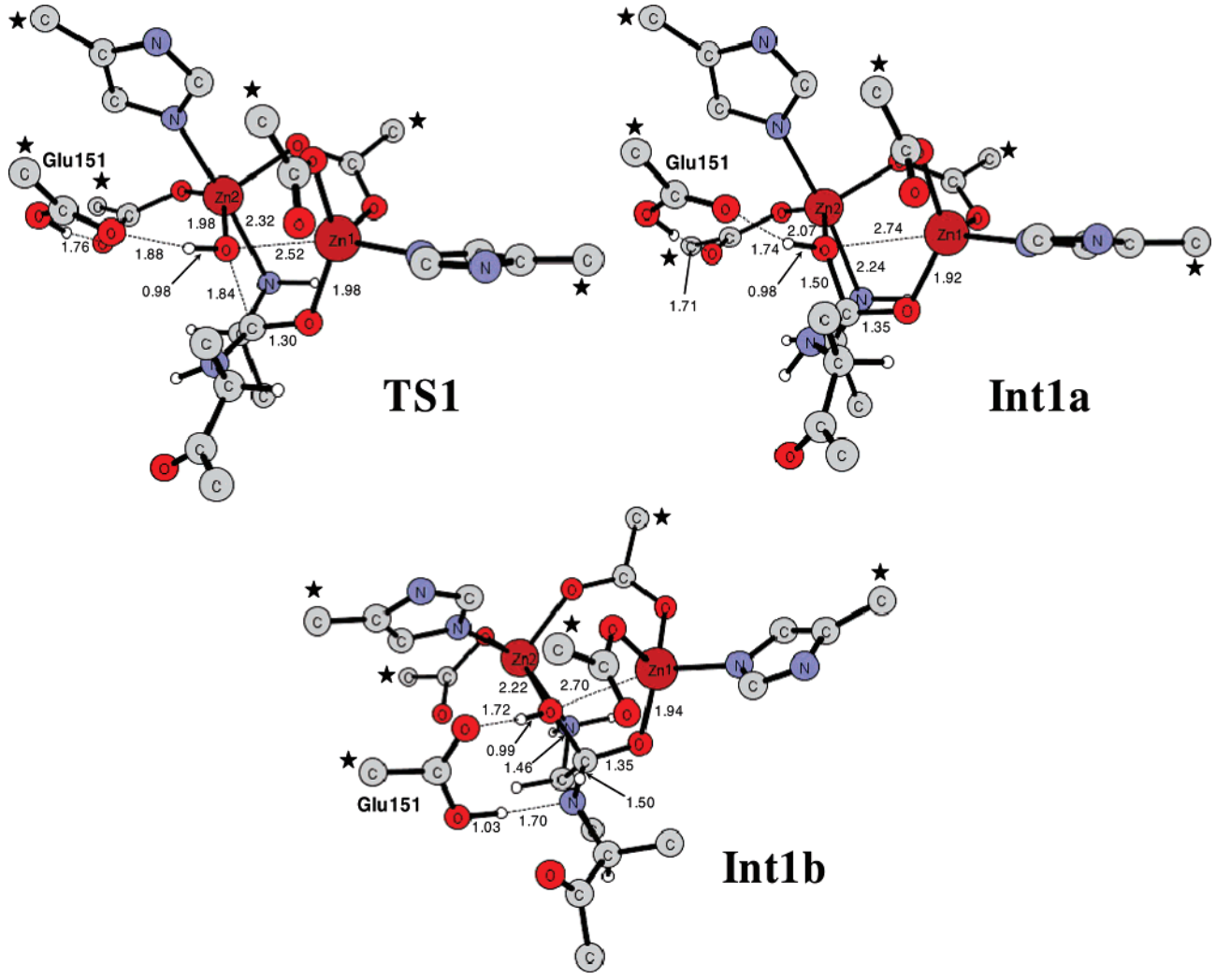

Figure 3. Optimized structures of the transition state for nucleophilic attack by $O_\mu H^-$ and the resulting intermediates.

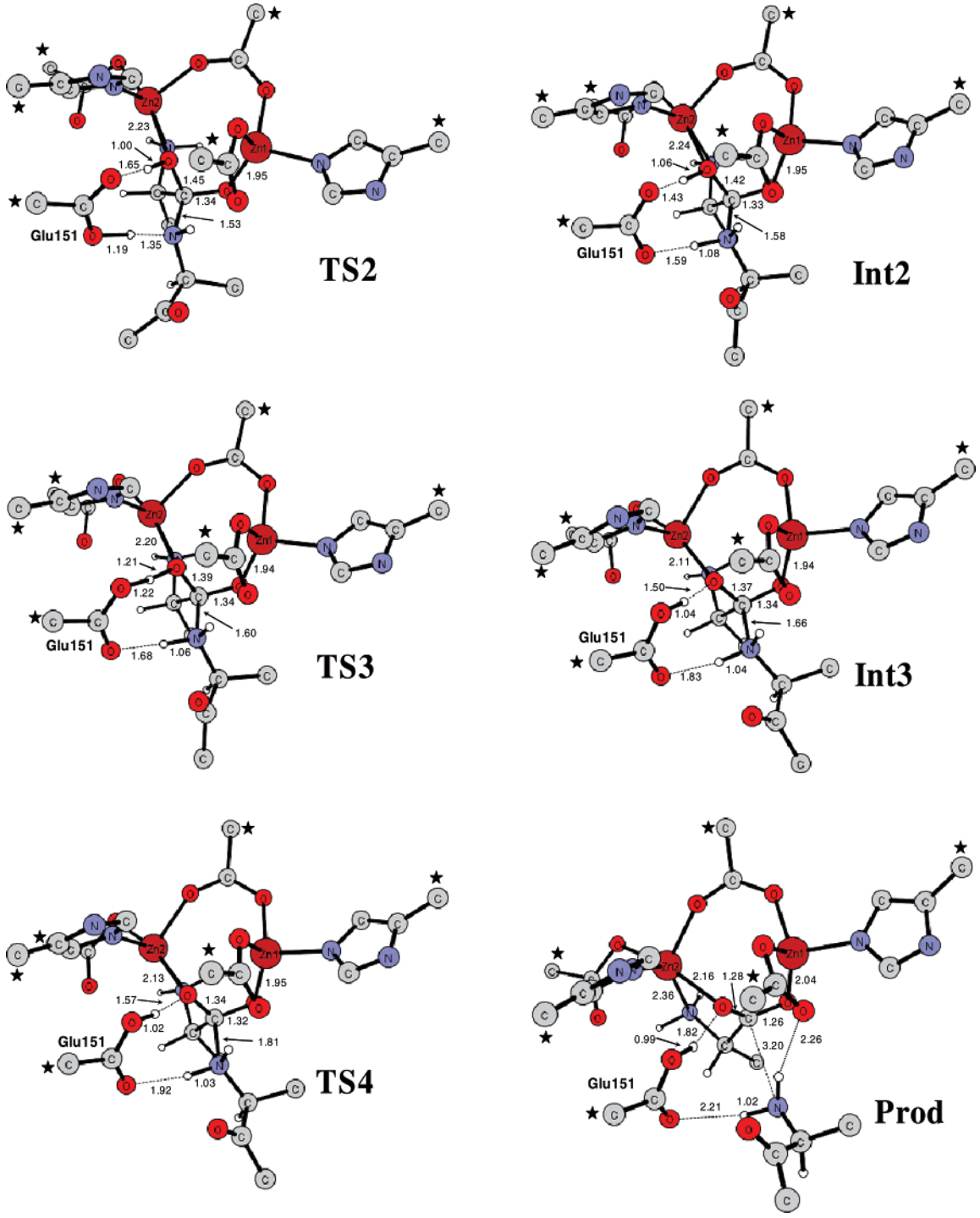

Figure 4. Optimized structures of transition states and intermediates along the reaction pathway.

of the carbonyl group to the same zinc less favorable as compared to the coordination of the amino group to Zn2, to which Asp179 is bound in a monodentate fashion. Similar results were obtained in the AM1/MM study.[23] One role of the Zn2 center seems thus to be to bind the substrate, assisting in orienting the peptide bond toward the nucleophile.

3.2. Nucleophilic Attack. It has been proposed that once the substrate is bound, the bridging hydroxide becomes terminal and then performs a nucleophilic attack on the carbonyl carbon of the peptide bond.[7,10,11,23] In **React**, the distance between the bridging oxygen and the carbonyl carbon of the peptide bond is 3.44 Å (Figure 2). We find that the attack happens directly from the bridging position and that the dissociation of the bridging hydroxide from Zn1 takes place simultaneously at the same transition state. The optimized transition state for this reaction step (**TS1**) and the resulting intermediate (**Int1a**) are displayed in Figure 3. The nature of **TS1** was confirmed to have an imaginary frequency of 186*i* cm^{-1}. The barrier is calculated to be the very feasible 12.1 kcal/mol in the cluster model. Upon the addition of surrounding solvation in the form of IEF-PCM, the barrier increases to 14.6 kcal/mol (i.e., the solvation energy of **React** is 2.5 kcal/mol larger than that for **TS1**). The intermediate is calculated to be 11.3 kcal/mol higher than the reactant (13.4 kcal/mol including solvation).

It is interesting to follow some geometrical changes that take place in going from **React** to **Int1a** via **TS1** (see Figures 2 and 3), as these can provide important chemical information. The peptide carbonyl double bond is elongated from 1.23 to 1.35 Å

SCHEME 2: Proposed Reaction Mechanism for AAP Based on Calculations in the Present Paper

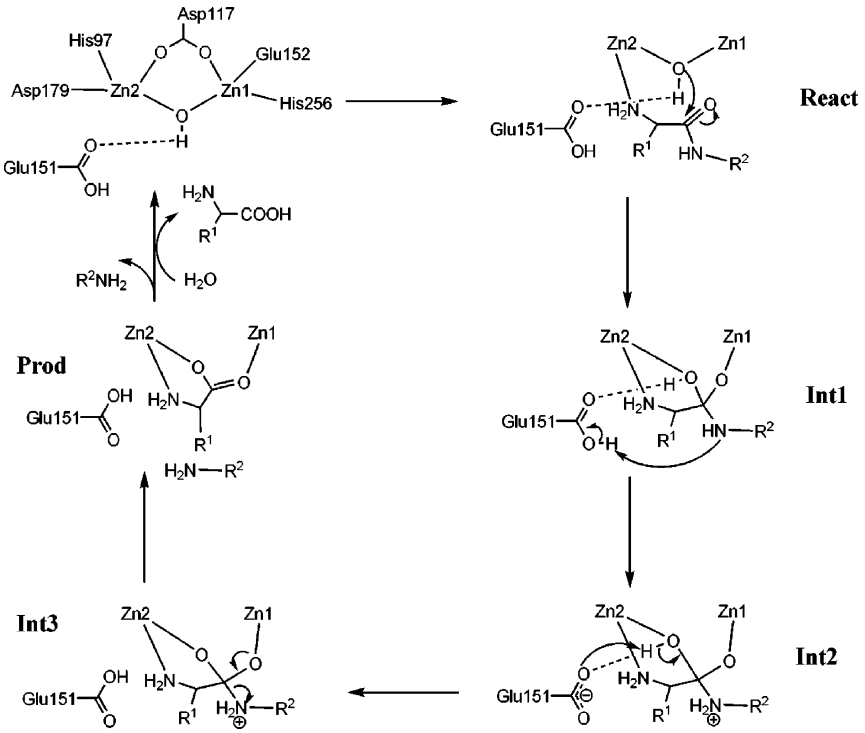

(1.30 Å at **TS1**), and the developing charge at the oxygen leads to its coordination to the Zn1 ion (1.98 Å in **TS1** and 1.92 Å in **Int1a**). This demonstrates that Zn1 provides catalytic power by stabilizing the developing negative charge of the oxygen atom of the tetrahedral intermediate. The bridging O_μ becomes terminal with distances of 2.07 Å to Zn2 and 2.74 Å to Zn1 in **Int1a**. The resulting gem-diolate moiety can thus be considered as a bridging ligand between the two Zn ions. The previous QM/MM investigation found this intermediate to be a bidentate ligand to the Zn1 ion.[23] The distance of Zn2 to the N-terminal nitrogen is also slightly shortened in the tetrahedral intermediate as compared to **React** (2.24 Å as compared to 2.37 Å), which indicates that the Zn2 ion, in addition to binding and orienting the substrate, might also contribute to the catalysis.

3.3. Proton Transfer. The second step in the hydrolysis reaction is the proton transfer from the Glu151 to the nitrogen of the peptide bond (N_P). To be able to do this, Glu151 has to rotate away from Asp179 and thus break its hydrogen bond to that residue. This rotation results in a new intermediate, denoted **Int1b**, which lies 4.1 kcal/mol higher than **Int1a** (structure displayed in Figure 3). We were not able to locate the transition state between **Int1a** and **Int1b**. However, since this step involves the rotation of a carboxylic group, and breaking a hydrogen bond and forming a new one, it is not expected to be substantially higher than the energy difference between the two hydrogen bonds (4.1 kcal/mol).

The transition states for the subsequent proton transfer (**TS2**) and the resulting intermediate (**Int2**) were optimized and are depicted in Figure 4. The nature of **TS2** was confirmed by a frequency calculation to have an imaginary frequency of 683*i* cm^{-1}. This proton transfer turns out to be the rate-limiting step for hydrolysis, with a barrier of 15.5 kcal/mol relative to the **React** species of Figure 2 (18.2 kcal/mol including solvation) (i.e., only less than 1 kcal/mol higher than **Int1b**). The resulting **Int2** intermediate lies 14.2 kcal/mol higher than the reactant (15.0 kcal/mol including solvation), which is 1.2 kcal/mol lower than **Int1b** (2.5 kcal/mol including solvation).

At **TS2**, the key distances of the proton to the peptide nitrogen and the Glu151 oxygen are 1.35 and 1.19 Å, respectively. In the intermediate species, the distance between the proton and the N_P is 1.08 Å. As the nitrogen becomes protonated, the C−N bond for the peptide is elongated from 1.50 to 1.58 Å (1.53 Å at **TS2**). Also, the hydrogen bond between Glu151 and $O_\mu H^-$ becomes stronger as Glu151 becomes anionic.

3.4. C−N Bond Cleavage. At **Int2**, the peptide bond is in principle ready to cleave. However, it turns out that another proton-transfer step must take place before the C−N bond can dissociate. Every attempt to locate a transition state for the C−N bond cleavage from **Int2** resulted in a transition state for a proton transfer from $O_\mu H^-$ to Glu151. In Figure 4, the optimized geometries of this transition state (**TS3**) and the resulting intermediate (**Int3**) are shown. **TS3** has been confirmed to be the first-order saddle point with an imaginary frequency of 510*i* cm^{-1}. **Int3** is only slightly more stable than **Int2** (0.1 kcal/mol in the cluster model and 0.6 kcal/mol including solvation). The barrier is calculated to be slightly negative (i.e., the energy of **TS3** is slightly lower than the energy for **Int2** (0.8 and 0.6 kcal/mol for the cluster model and including solvation, respectively)). This is of course an error in the methods and models employed. When the real barrier is very low, like in this case, a small underestimation in the calculated barrier can yield artificially slightly negative barriers. The firm conclusion, however, is that this step is very fast. At **TS3**, the distances of the proton to the O_μ and Glu151 oxygen are 1.21 and 1.22 Å, respectively. With the proton delivered to Glu151, the bond of O_μ to the peptide carbon (C_P) is shortened from 1.42 to 1.37 Å, and the C_P-N_P bond is elongated from 1.58 to 1.66 Å.

From **Int3**, a transition state for the C−N bond cleavage could be located (**TS4**, shown in Figure 4) and was calculated to have an imaginary frequency of 104*i* cm^{-1}. Also for this step, the barrier is calculated to be slightly negative (ca 0.6 kcal/mol), which again is an error in the methods but which shows that the step is very fast. The C−N bond distance at the transition state is 1.81 Å.

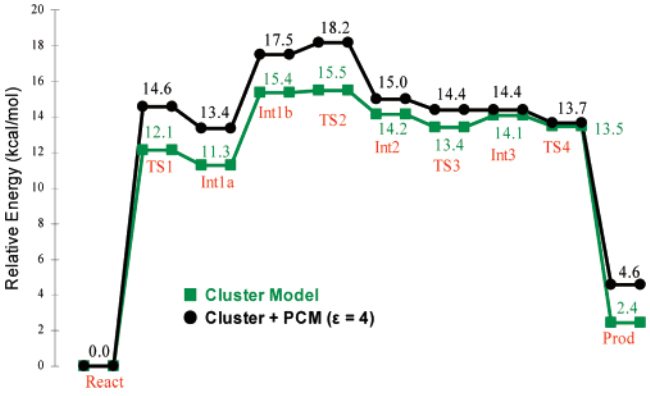

Figure 5. Calculated potential energy profile for peptide hydrolysis by AAP. (Cluster) B3LYP/6-311+G(2d,2p) energies with zero-point energies included. (PCM) IEF-PCM solvation effects added with dielectric constant $\epsilon = 4$.

The C−N bond cleavage leads to a neutral amino group that dissociates and a deprotonated carboxylate moiety that is bridging the two zinc ions (see Figure 4, **Prod**). In the cluster model, the energy of this species is 2.4 kcal/mol higher than that for the reactant species of Figure 2 (+4.6 kcal/mol when solvation is added). It should be mentioned that several attempts were made to find a concerted transition state (i.e., proton transfer from Glu151 coupled with the C−N bond cleavage) but without success.

4. Conclusion

In this paper, we have reported a theoretical examination of the peptide hydrolysis mechanism of an aminopeptidase from AAP. A model of the active site was built on the basis of the X-ray crystal structure, and a model dipeptide was chosen as a substrate. Transition states and intermediates along the reaction pathway were located and characterized. The obtained reaction mechanism is shown in Scheme 2, and the associated calculated energetic profile is presented in Figure 5.

With the help of the calculations, the following mechanistic features were established. First, the substrate was found to bind to the di-zinc cluster through the amino group and not the peptide carbonyl. The Zn2 ion thus has an important role in binding the substrate and orienting the peptide bond toward the nucleophile. The calculations furthermore demonstrate that the bridging hydroxide is capable of performing a nucleophilic attack at the peptide carbonyl without the need to become terminal. This conclusion is of importance for a number of other hydrolytic di-zinc enzymes.[29] The main catalytic power originates from the Zn1 ion, which stabilizes the anionic tetrahedral intermediate, thereby lowering the barrier for the nucleophilic attack. The rate-limiting step was found to be the proton transfer from Glu151 to the nitrogen of the peptide bond, with an accumulated barrier of 18.2 kcal/mol. This is consistent with the experimental finding that the rate-limiting step involves a proton transfer.[13,19] After that, two very fast steps took place to complete the hydrolysis, namely, a proton transfer from $O_\mu H^-$ to Glu151 and C−N bond cleavage. The barriers and intermediate energies of the last two steps are, however, such that it cannot be excluded that they occur concertedly with the first rate-limiting proton transfer from Glu151 to the nitrogen of the peptide bond.

Finally, the results of this paper testify to the usefulness of accurate quantum chemical active site models to investigate mechanistic proposal of enzymes. In particular, the small difference in the potential energy profile for the cluster model with and without continuum solvation (on the order of 2−3 kcal/mol; see Figure 5) indicates that most of the polarization is captured already by the cluster model, yielding further validation for this kind of model.

Acknowledgment. Financial support from the Università degli Studi della Calabria and Regione Calabria (POR Calabria 2000/2006, Misura 3.16, Progetto PROSICA) is gratefully acknowledged. F.H. gratefully acknowledges financial support from The Swedish National Research Council, The Wenner-Gren Foundations, The Carl Trygger Foundation, and The Magn Bergvall Foundation. This work was also supported by grant from the Major State Basic Research Development Programs (Grant 2004CB719903) to W.-H.F.

Supporting Information Available: Table with geometrical parameters for various structures. Cartesian coordinates of all optimized structures. This material is available free of charge via the Internet at http://pubs.acs.org.

References and Notes

(1) Wilcox, D. E. *Chem. Rev.* **1996**, *96*, 2435.
(2) Lowther, W. T.; Matthews, B. W. *Chem. Rev.* **2002**, *102*, 4581.
(3) Prescott, J. M.; Wilkes, S. H.; Wagner, F. W.; Wilson, K. J. *J Biol. Chem.* **1971**, *246*, 1756.
(4) Prescott, J. M.; Wilkes, S. H. *Methods Enzymol.* **1976**, *45*, 530.
(5) Holz, R. C. *Coord. Chem. Rev.* **2002**, *232*, 5.
(6) Wagner, F. W.; Wilkes, S. H.; Prescott, J. M. *J. Biol. Chem.* **1972**, *247*, 1208.
(7) Chen, G.; Edwards, T.; D'souza, V. M.; Holz, R. C. *Biochemistry* **1997**, *36*, 4278.
(8) Chevrier, B.; Schalk, C.; D'Orchymont, H.; Rondeau, J.-M.; Moras, D.; Tarnus, C. *Structure* **1994**, *2*, 283.
(9) Chevrier, B.; D'Orchymont, H.; Schalk, C.; Tarnus, C.; Moras, D. *Eur. J. Biochem.* **1996**, *237*, 393.
(10) De Paola, C. C.; Bennett, B.; Holz, R. C.; Ringe, D.; Petsko, G. A. *Biochemistry* **1999**, *38*, 9048.
(11) Stamper, C.; Bennett, B.; Edwards, T.; Holz, R. C.; Ringe, D.; Petsko, G. *Biochemistry* **2001**, *40*, 7035.
(12) Desmarais, W. T.; Bienvenue, D. L.; Bzymek, K. P.; Holz, R. C.; Petsko, G. A.; Ringe, D. *Structure* **2002**, *10*, 1063.
(13) Bzymek, K. P.; Moulin, A.; Swierczek, S. I.; Ringe, D.; Petsko, G. A.; Bennett, B.; Holz, R. C. *Biochemistry* **2005**, *44*, 12030.
(14) Desmarais, W.; Bienvenue, D.; Bzymek, K. P.; Petsko, G. A.; Ringe, D.; Holz, R. C. *J. Biol. Inorg. Chem.* **2006**, *11*, 398.
(15) Ustynyuk, L.; Bennett, B.; Edwards, T.; Holz, R. C. *Biochemistry* **1999**, *38*, 11433.
(16) Bennett, B.; Holz, R. C. *J. Am. Chem. Soc.* **1997**, *119*, 1923.
(17) Bennett, B.; Holz, R. C. *Biochemistry* **1997**, *36*, 9837.
(18) Bzymek, K. P.; Holz, R. C. *J. Biol. Chem.* **2004**, *279*, 31018.
(19) Bienvenue, D. L.; Mathew, R. S.; Ringe, D.; Holz, R. C. *J. Biol. Inorg. Chem.* **2002**, *7*, 129.
(20) Bennett, B.; Holz, R. C. *J. Am Chem. Soc.* **1998**, *120*, 12139.
(21) Bzymek, K. P.; Swierczek, S. I.; Bennett, B.; Holz, R. C. *Inorg. Chem.* **2005**, *44*, 8574.
(22) Bienvenue, D. L.; Gilner, D.; Holz, R. C. *Biochemistry* **2002**, *41*, 3712.
(23) Schürer, G.; Lanig, H.; Clark, T. *Biochemistry* **2004**, *43*, 5414.
(24) (a) Becke, A. D. *J. Chem. Phys.* **1993**, *98*, 1372. (b) Becke, A. D. *J. Chem. Phys.* **1993**, *98*, 5648. (c) Lee, C.; Yang, W.; Parr, R. G. *Phys. Rev. B: Condens. Matter Mater. Phys.* **1988**, *37*, 785.
(25) (a) Himo, F.; Siegbahn, P. E. M. *Chem. Rev.* **2003**, *103*, 2421. (b) Siegbahn, P. E. M. *Q. Rev. Biophys.* **2003**, *36*, 91. (c) Noodleman, L.; Lovell, T.; Han, W.-G.; Li, J.; Himo, F. *Chem. Rev.* **2004**, *104*, 459. (d) Siegbahn, P. E. M.; Borowski, T. *Acc. Chem. Res.* **2006**, *39*, 729. (e) Himo, F. *Theor. Chem. Acc.* **2006**, *116*, 232. (f) Marino, T.; Russo, N.; Toscano, M. *J. Am. Chem. Soc.* **2005**, *127*, 4242. (g) Leopoldini, M.; Russo, N.; Toscano, M.; Dulak, M.; Wesoloski, A. T. *Chem.—Eur. J.* **2006**, *12*, 2532. (h) Leopoldini, M.; Russo, N.; Toscano, M. *J. Phys. Chem. B* **2006**, *110*, 1063. (i) Chen, S.-L.; Fang, W.-H.; Himo, F. *J. Phys. Chem. B* **2007**, *111*, 1253.
(26) (a) Fuentealba, P.; Preuss, H.; Stoll, H.; Szentpaly, L. V. *Chem. Phys. Lett.* **1989**, *89*, 418. (b) Szentpaly, L. V.; Fuentealba, P.; Preuss, H.; Stoll, H. *Chem. Phys. Lett.* **1982**, *93*, 555. (c) Fuentealba, P.; Stoll, H.; Szentpaly, L. V.; Schwerdtfeger, P.; Preuss, H. *J. Phys. B* **1983**, *16*, 1323. (d) Stoll, H.; Fuentealba, P.; Schwerdtfeger, P.; Flad, J.; Szentpaly, L. V.; Preuss, H. *J. Chem. Phys.* **1984**, *81*, 2732. (e) Dolg, M.; Wedig, U.; Stoll, H.; Preuss, H. *J. Chem. Phys.* **1987**, *86*, 866.

(27) (a) Cancès, M. T.; Mennucci, B.; Tomasi, J. *J. Chem. Phys.* **1997**, *107*, 3032. (b) Cossi, M.; Barone, V.; Mennucci, B.; Tomasi, J. *Chem. Phys. Lett.* **1998**, *286*, 253. (c) Mennucci, B.; Tomasi, J. *J. Chem. Phys.* **1997**, *106*, 5151. (d) Mennucci, B.; Cancès, E.; Tomasi, J. *J. Phys. Chem. B* **1997**, *101*, 10506.

(28) Frisch, M. J.; Trucks, G. W.; Schlegel, H. B.; Scuseria, G. E.; Robb, M. A.; Cheeseman, J. R.; Montgomery, J. A., Jr.; Vreven, T.; Kudin, K. N.; Burant, J. C.; Millam, J. M.; Iyengar, S. S.; Tomasi, J.; Barone, V.; Mennucci, B.; Cossi, M.; Scalmani, G.; Rega, N.; Petersson, G. A.; Nakatsuji, H.; Hada, M.; Ehara, M.; Toyota, K.; Fukuda, R.; Hasegawa, J.; Ishida, M.; Nakajima, T.; Honda, Y.; Kitao, O.; Nakai, H.; Klene, M.; Li, X.; Knox, J. E.; Hratchian, H. P.; Cross, J. B.; Bakken, V.; Adamo, C.; Jaramillo, J.; Gomperts, R.; Stratmann, R. E.; Yazyev, O.; Austin, A. J.; Cammi, R.; Pomelli, C.; Ochterski, J. W.; Ayala, P. Y.; Morokuma, K.; Voth, G. A.; Salvador, P.; Dannenberg, J. J.; Zakrzewski, V. G.; Dapprich, S.; Daniels, A. D.; Strain, M. C.; Farkas, O.; Malick, D. K.; Rabuck, A. D.; Raghavachari, K.; Foresman, J. B.; Ortiz, J. V.; Cui, Q.; Baboul, A. G.; Clifford, S.; Cioslowski, J.; Stefanov, B. B.; Liu, G.; Liashenko, A.; Piskorz, P.; Komaromi, I.; Martin, R. L.; Fox, D. J.; Keith, T.; Al-Laham, M. A.; Peng, C. Y.; Nanayakkara, A.; Challacombe, M.; Gill, P. M. W.; Johnson, B.; Chen, W.; Wong, M. W.; Gonzalez, C.; Pople, J. A. *Gaussian 03*, revision C.02; Gaussian, Inc.: Pittsburgh, PA, 2004.

(29) (a) Weston, J. *Chem. Rev.* **2005**, *105*, 2151. (b) Seibert, C. M.; Raushel, F. M. *Biochemistry* **2005**, *44*, 6383.